

Ferro-papikeite, ideally $\text{NaFe}_2^{2+}(\text{Fe}_3^{2+}\text{Al}_2)(\text{Si}_5\text{Al}_3)\text{O}_{22}(\text{OH})_2$, a new orthorhombic amphibole from Nordmark (Western Bergslagen), Sweden: Description and crystal structure

FRANK C. HAWTHORNE^{1,*}, MAXWELL C. DAY¹, MOSTAFA FAYEK¹, KEES LINTHOUT²,
WIM. J. LUSTENHOUWER², AND ROBERTA OBERTI³

¹Department of Earth Sciences, University of Manitoba, Winnipeg, Manitoba R3T 2N2, Canada

²Geology & Geochemistry Research Cluster, Vrije Universiteit, Amsterdam, The Netherlands

³CNR-Istituto di Geoscienze e Georisorse, sede secondaria di Pavia, via Ferrata 1, I-27100 Pavia, Italy

ABSTRACT

Ferro-papikeite, ideally $\text{NaFe}_2^{2+}(\text{Fe}_3^{2+}\text{Al}_2)(\text{Si}_5\text{Al}_3)\text{O}_{22}(\text{OH})_2$, is a new mineral of the amphibole supergroup from the Filipstad Municipality, Värmland County, Central Sweden, where it occurs in a medium-grade felsic metavolcanic rock. Ferro-papikeite is pale brown with a translucent luster, has a colorless to very pale-brown streak, and shows no fluorescence under long-wave or short-wave ultraviolet light. Grains are subhedral, 0.4–3.0 mm in size, and show well-developed {210} cleavage. It has a Mohs hardness of ~6 and is brittle with a splintery fracture, has the characteristic perfect {210} cleavage of orthorhombic amphiboles, intersecting at ~56°, and the calculated density is 3.488 g/cm³. In transmitted plane-polarized light, ferro-papikeite is moderately pleochroic X = very pale brown, Y = Z = honey brown; X < Y = Z. Ferro-papikeite is biaxial (+), $\alpha = 1.674(2)$, $\beta = 1.692(2)$, $\gamma = 1.716(2)$, $2V_{\text{meas}} = 86.2(9)$ and $2V_{\text{calc}} = 88.3^\circ$, dispersion is $r < v$, weak. The orientation is: X || a, Y || b, Z || c.

Ferro-papikeite is orthorhombic, space group *Pnma*, $a = 18.628(4)$, $b = 17.888(4)$, $c = 5.3035(11)$ Å, $V = 1767.2(6)$ Å³, $Z = 4$. The strongest ten X-ray diffraction lines in the powder pattern are [d in Å(hkl)]: 8.255(100)(210), 3.223(39)(440), 3.057(68)(610), 2.824(28)(251), 2.674(41)(351), 2.572(56)(161,621), 2.549(38)(202), 2.501(50)(261,451), 2.158(25)(502), and 1.991(31)(661). Chemical analysis by electron microprobe gave SiO₂ 36.50, Al₂O₃ 22.24, TiO₂ 0.09, FeO 31.54, MnO 0.65, MgO 5.48, CaO 0.08, Na₂O 2.35, F 0.22, H₂O_{calc} 1.85, O=F -0.09, sum 100.91 wt%. The formula unit, calculated on the basis of 24 (O+OH+F) with (OH) = 2 apfu and Fe³⁺ = 0.13 apfu (determined from the <M2–O> distance) is ^A(Na_{0.70}Ca_{0.01})^{B+C}(Mg_{1.25}Fe_{3.90}Mn_{0.08}Al_{1.62}Fe_{0.13}Ti_{0.01})_{Σ6.99}^T(Si_{5.60}Al_{2.40})_{Σ8}O₂₂(OH_{1.89}F_{0.11})₂. The crystal structure of ferro-papikeite was refined to an R-index of 3.60% using 2335 unique observed reflections collected with MoK α X-radiation. ¹⁴Al³⁺ is ordered over the four T sites as follows: T1B > T1A > T2B >> T2a, ¹⁶Al³⁺ is completely ordered at M2, and Fe²⁺ is strongly ordered at M4. The A site is split with Na⁺ strongly ordered at A1. End-member ferro-papikeite is related to end-member gedrite, □Mg₂(Mg₃Al₂)(Si₆Al₂)O₂₂(OH)₂, by the substitutions Na⁺ → □, Fe²⁺ → Mg, and Al³⁺ → Si⁴⁺. The description of ferro-papikeite as a new species further emphasizes the compositional similarities between the monoclinic calcium amphiboles and the orthorhombic magnesium-iron-manganese amphiboles.

Keywords: Ferro-papikeite, new amphibole, electron-microprobe analysis, optical properties, crystal-structure refinement, Bergslagen, Sweden

INTRODUCTION

The general chemical formula of the amphiboles may be written (Hawthorne and Oberti 2007) as



where A = Na⁺, K⁺, □, Ca²⁺, Li⁺;

B = Na⁺, Li⁺, Ca²⁺, Mn²⁺, Fe²⁺, Mg²⁺;

C = Mg²⁺, Fe²⁺, Mn²⁺, Al³⁺, Fe³⁺, Mn³⁺, Ti⁴⁺, Li⁺;

T = Si⁴⁺, Al³⁺, Ti⁴⁺;

W = (OH), F, Cl, O²⁻.

Rabbitt (1948) reviewed all previous work on orthorhombic amphiboles and described their composition as varying from Mg₇Si₈O₂₂(OH)₂ to Mg₅Al₂Si₆Al₂O₂₂(OH)₂. Robinson and Jaffe (1969) and Robinson et al. (1971) showed that Na is an essential constituent of gedritic amphiboles, and Papike and Ross (1970)

refined the structures of two gedrites and located Na at the A-site between the back-to-back ribbons of (Si,Al)O₄ tetrahedra. Robinson and Jaffe (1969) and Ross et al. (1969) found that amphiboles intermediate in composition between anthophyllite and gedrite are unmixed at the microscopic or submicroscopic scale along lamellae parallel to (010), and Stout (1971) confirmed the presence of a solvus by finding coarse coexisting orthorhombic amphiboles. Schindler et al. (2008) and Hawthorne et al. (2008) refined the crystal structures of 25 anthophyllite-gedrite amphiboles mainly from amphibolite-facies rocks and showed that their compositions closely follow the linear relation outlined by Robinson et al. (1971) from ideal anthophyllite to the composition Na_{0.5}M₂²⁺(M_{3.5}³⁺M_{1.5}⁴⁺)(Si₆Al₂)O₂₂(OH)₂ where M²⁺ = Mg²⁺, Fe²⁺; M³⁺ = Al³⁺, Fe³⁺ (Ti⁴⁺). Only six of their compositions equaled or exceeded 0.50 Na pfu (per formula unit) (maximum value = 0.56, mean value = 0.52 Na pfu). When the current amphibole nomenclature scheme was developed (Hawthorne et

* E-mail: frank.hawthorne@umanitoba.ca

al. 2012), *Pnma* amphiboles with compositions >0.5 Na pfu had not been approved by IMA-CNMMN as distinct mineral species, and hence such compositions were assigned the temporary names Rootname 1: $\text{NaMg}_2\text{Mg}_5(\text{Si}_7\text{Al})\text{O}_{22}(\text{OH})_2$ and Rootname 2: $\text{NaMg}_2(\text{Mg}_3\text{Al}_2)(\text{Si}_5\text{Al}_3)\text{O}_{22}(\text{OH})_2$, to be replaced by suitable rootnames when submitted for approval. Berg (1985) showed that Na may reach close to 1 atoms per formula unit (apfu) for compositions close to $^{|\text{Al} + \text{Fe}^{3+} + 2\text{Ti}|} = 1$ apfu, but there was no structural information on these compositions. Linthout and Lustenhouwer (1996) reported subsilicic “sodium gedrite,” as classified under then prevailing IMA rules (Leake 1978), an orthorhombic amphibole with a composition close to the center of the composition field of Rootname 2. This amphibole has now been characterized as a new mineral species and has been named ferro-papikeite, the prefix “ferro-” being dictated by the current amphibole nomenclature scheme as $^{\text{cFe}^{2+}} > ^{\text{cMg}^{2+}}$. The rootname “papikeite” is after James J. Papike, born February 11, 1937, in Eveleth, Minnesota, U.S.A., died 21 December 2020. Jim Papike was a prominent America crystallographer and geochemist, one of the “fathers” of petrological crystal-chemistry who did a lot of crystallographic work on amphiboles, and orthorhombic

amphiboles in particular, in the second half of the 1960s and the early 1970s, and whose work catalyzed renewed interest in amphiboles at that time. Jim Papike was also well-known for his extensive work on lunar petrology and geochemistry.

The new species and the new name have been approved by the International Mineralogical Association Commission on New Minerals, Nomenclature and Classification (2020-021). Holotype material is deposited in the mineral collection of the Department of Natural History, Royal Ontario Museum, Canada, catalog number M60100.

OCCURRENCE

Ferro-papikeite was found in the Filipstad Municipality, Värmland County, Central Sweden (the western part of the Bergslagen Ore Province); Mapsheet 11E, Filipstad NV 6640.00/1403.42 (RT90 National Swedish Topographic Net), N 59°50'37.53" E 14°06'3.49", in a medium-grade, felsic metavolcanic rock. Ferro-papikeite occurs as isolated subhedral grains (Figs. 1a and 1b), 0.4–3.0 mm in size, and as sheaf-like bundles of subhedral prisms up to 4 mm in size intergrown with biotite and chlorite (Figs. 1c and 1d) in a fine-grained matrix of anhedral quartz, albite, biotite, and

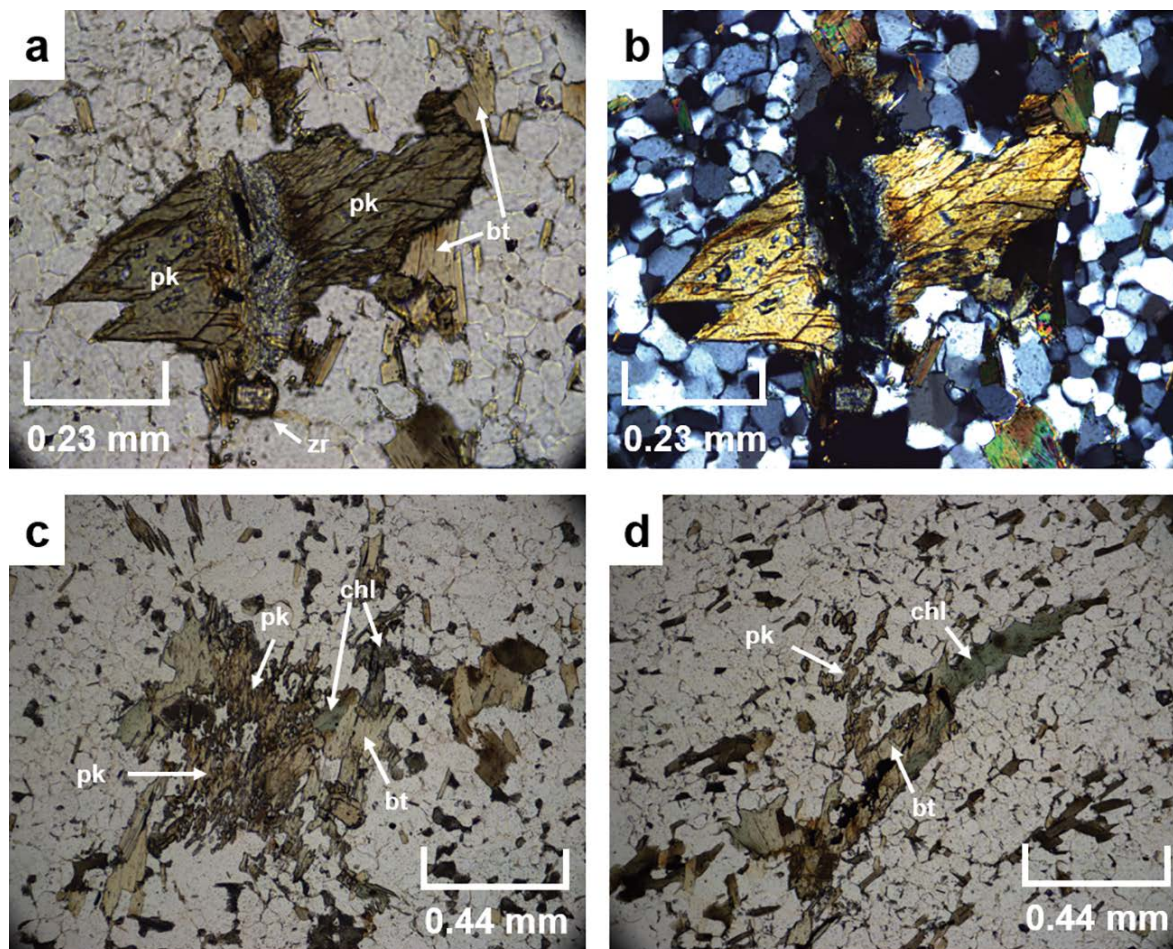


FIGURE 1. Thin section of the felsic metavolcanic rock that contains (a) a large isolated crystal of ferro-papikeite viewed down the c-axis, showing well-developed {210} cleavage and set in a fine-grained matrix of quartz, albite, biotite, and chlorite (viewed in plane-polarized light); (b) the same crystal viewed in cross-polarized light; (c and d) sheaf-like bundles of ferro-papikeite prisms intergrown with biotite and chlorite. Legend: pk = ferro-papikeite, bt = biotite, chl = chlorite, zr = zircon.

chlorite, in which biotite and stretched quartz phenocrysts define a weak-to-moderate foliation (Fig. 2a). K-feldspar phenocrysts have been partly to completely albitized and show Carlsbad-twinning (Fig. 2b). Several different deformation textures are observed in both K-feldspar and quartz phenocrysts (Figs. 2c–2f). Chlorite occurs as subhedral plates and as very fine-grained aggregates partly replacing biotite and ferro-papikeite (Figs. 1c and 1d).

PETROLOGICAL SETTING

Widespread andalusite and cordierite porphyroblasts in metasediments (Magnusson 1970) locally preserve microscopic sedimentary textures (Roep and Linthout 1989) and indicate medium-grade (lower amphibolite facies) regional but static low-pressure metamorphism in the Nordmark area. Ferro-papikeite occurs in a fine-grained (~0.1 mm) granoblastic quartz-albite matrix that has undergone moderate deformation and recrystallization, resulting in an overall polygonal texture. Quartz and albite are also present as millimeter-sized pseudomorphs after phenocrysts of quartz and feldspar. Quartz phenocrysts show undulatory extinction and significant subgrain development and rotation (Fig. 2c). Albite phenocrysts also show subgrain development via grain-boundary migration and bulging, and deformation-related tapered twinning is also present (Figs. 2d–2f). Such textures indicate that plagioclase and alkali feldspar have undergone significant recrystallization, indicative of metamorphic conditions of $\geq 500^\circ\text{C}$.

Brown biotite flakes (≤ 0.4 mm) occur intergrown with ferro-papikeite and dispersed in the matrix. Subordinate ilmenite and

zircon form platelets ≥ 0.1 mm and euhedral crystals ≥ 0.2 mm in size, respectively (Fig. 1). Ferro-papikeite and biotite are partly replaced by chlorite (Figs. 1c and 1d) and some isolated ferro-papikeite grains are altered and appear “cross-cut” by very fine-grained aggregates of chlorite (Figs. 1a and 1b). This suggests two dominant metamorphic events; the first is associated with the crystallization of ferro-papikeite and the second is associated with the replacement (alteration) of biotite and ferro-papikeite by chlorite.

The abundance of phenocrystic quartz in the silica-rich leptite suggests a rhyolitic origin. However, the CaO and K_2O contents are significantly below the average values typical for pristine rhyolites, and the FeO and MgO contents are relatively high (Table 1). Considering that synvolcanic sub-seafloor hydrothermal alteration is widespread in the supracrustal precursor rocks of western Bergslagen (Lagerblad and Gorbatshev 1985), the protolith of the host rock can best be described as a quartz keratophyre, a common rock-type in low-grade metamorphic areas of Bergslagen (Linthout 1983). Mutatis mutandis, the protolith’s characteristics are highly compatible with the generally accepted view that many orthoamphibole-cordierite/(staurolite)-bearing rocks are metamorphosed spilites (Vallance 1967; Spear 1993).

PHYSICAL AND OPTICAL PROPERTIES

Ferro-papikeite is pale brown with a translucent luster. It has a colorless to very pale brown streak and shows no fluorescence under long-wave or short-wave ultraviolet light. Grains are

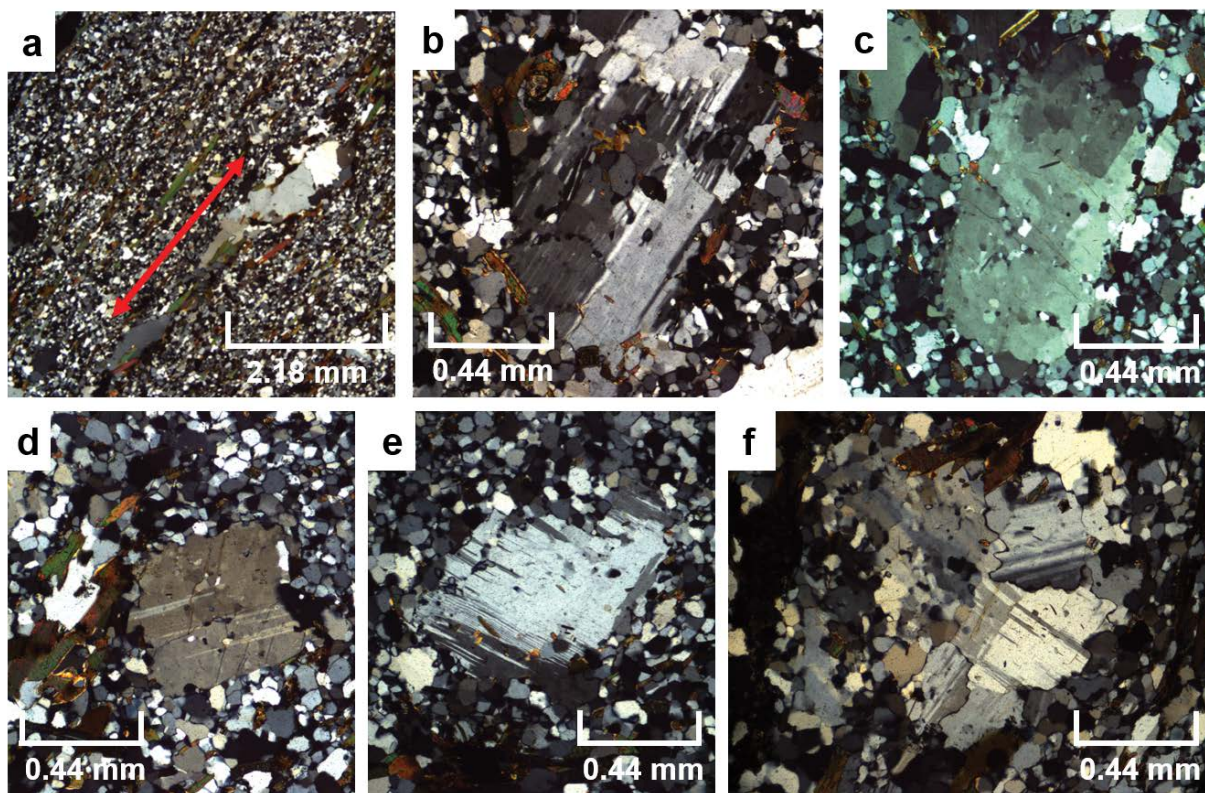


FIGURE 2. Thin section (viewed in cross-polarized light) of (a) the fine-grained matrix showing a weak-to-moderate foliation defined by biotite and elongate quartz phenocrysts (red arrow shows foliation direction); (b) Carlsbad twinning in an albite phenocryst; (c) quartz phenocryst showing undulatory extinction and subgrain development; (d, e, and f) albite phenocrysts showing subgrain development via grain boundary migration and bulging, and tapered twinning.

TABLE 1. Composition of leptite from Nordmark

	Leptite LT78B2	Average ^a rhyolite
SiO ₂	77.4	72.82
TiO ₂	0.17	0.27
Al ₂ O ₃	11.52	13.53
Fe ₂ O ₃	–	1.48
FeO	3.87	1.11
MnO	0.03	0.06
MgO	1.31	0.39
CaO	0.19	1.14
Na ₂ O	3.78	3.55
K ₂ O	0.81	4.30
P ₂ O ₅	0.03	0.07
H ₂ O ⁺	–	1.10
H ₂ O [–]	–	0.31
CO ₂	–	0.08
Sum	99.11	99.96

^a From Le Maitre (1976).

subhedral, 0.4–3.0 mm in size, and show well-developed {210} cleavage intersecting at ~56° (Fig. 2). Ferro-papikiteite has a Mohs hardness of ~6 and is brittle with a splintery fracture; the calculated density is 3.488 g/cm³.

In transmitted plane-polarized light ($\lambda = 590$ nm), ferro-papikiteite is moderately pleochroic X = very pale brown, Y = Z = honey brown; X < Y = Z. A spindle stage was used to orient a crystal for measurement of refractive indices in white light and 2*V* by extinction curves (Bartelmehs et al. 1992). Ferro-papikiteite is biaxial (+), $\alpha = 1.674(2)$, $\beta = 1.692(2)$, $\gamma = 1.716(2)$, $2V_{\text{meas}} = 86.2(9)$ and $2V_{\text{calc}} = 88.3^\circ$, dispersion is $r < v$, weak. The orientation is: X || a, Y || b, Z || c.

CHEMICAL COMPOSITION

Ferro-papikiteite was analyzed by electron microprobe using a Cameca SX-100 operating in wavelength-dispersive mode with excitation voltage 15 kV, specimen current 20 nA, beam diameter 10 μm , peak-count time 20 s, and background-count time 10 s for all elements except F for which a peak-count time of 30 s and a background-count time of 15 s was used. The following standards and crystals were used for *K α* X-ray lines: Si: almandine, TAP; Ca: diopside, TAP, LPET; Ti: titanite, LPET; Fe: fayalite, LLiF; Mn: spessartine, LLiF; Mg: forsterite, TAP; Na: albite, TAP; Al: andalusite, TAP. Data reduction was done using the $\phi(\rho Z)$ procedure of Pouchou and Pichoir (1985). The average of 10 analyses on a single grain is given in Table 2. The Fe³⁺ content of anthophyllite-gedrite amphiboles is very low. We determined Fe³⁺ as 0.13 apfu from the observed <M2–O> bond length and the mean bond-length – mean cation-radius curve of Schindler et al. (2008), close to the mean Fe²⁺/(Fe²⁺+Fe³⁺) value of 0.96 for 25 anthophyllite-gedrite amphiboles reported by Schindler et al. (2008).

The empirical chemical formula, calculated on the basis of 24 (O+OH+F) with OH+F = 2 apfu and Fe³⁺ = 0.13 apfu, is as follows: (Na_{0.70}Ca_{0.01})(Mg_{1.25}Fe_{3.90}Mn_{0.08}Al_{1.62}Fe_{0.13}Ti_{0.01})_{Σ6.99}(Si_{5.60}Al_{2.40})_{Σ8}O₂₂(OH_{1.89}F_{0.11})₂. The simplified formula is: (Na,□)_{Σ1}(Fe,Mg,Al)_{Σ7}(Si,Al)_{Σ8}O₂₂(OH)₂ and the ideal formula is: NaFe₃²⁺(Fe₃²⁺Al₂)(Si₅Al₃)O₂₂(OH)₂, which requires Na₂O 3.22, FeO 37.28, Al₂O₃ 26.45, SiO₂ 31.18, H₂O 1.87, total 100 wt%.

X-ray powder diffraction

As ferro-papikiteite is intergrown with, or partly replaced by biotite and chlorite, it was not possible to get sufficient pure

TABLE 2. Chemical composition (wt%) and unit formula (apfu) for ferro-papikiteite

SiO ₂	36.50	Si ⁴⁺	5.60
TiO ₂	0.09	Al ³⁺	2.40
Al ₂ O ₃	22.24	ΣT	8.00
Fe ₂ O ₃	1.15	Al ³⁺	1.62
FeO	30.50	Ti ⁴⁺	0.01
MnO	0.65	Fe ³⁺	0.13
MgO	5.48	Fe ²⁺	3.90
CaO	0.08	Mn ²⁺	0.08
Na ₂ O	2.35	Mg ²⁺	1.25
F	0.22	ΣB+C	6.99
O=F	–0.09	Ca ²⁺	0.01
H ₂ O	1.85	Na ⁺	0.70
Total	100.88	(OH) [–]	1.89
		F [–]	0.11

TABLE 3. X-ray powder diffraction for ferro-papikiteite

<i>l</i>	<i>d</i> (Å)	<i>hkl</i>	<i>l</i>	<i>d</i> (Å)	<i>hkl</i>
15	8.9371	0 2 0	8	2.4144	6 5 0
99	8.2553	2 1 0	19	2.3185	5 5 1
6	5.0178	2 3 0	8	2.2974	7 2 1
14	4.6528	4 0 0	"	"	6 4 1
8	4.6094	2 0 1	6	2.2840	4 1 2
9	4.0944	2 2 1	"	"	1 7 1
8	3.9501	1 3 1	7	2.2340	0 8 0
18	3.6436	2 3 1	"	"	2 7 1
10	3.3378	3 3 1	25	2.1583	5 0 2
"	"	2 5 0	19	2.1421	5 1 2
39	3.2231	4 4 0	"	"	3 4 1
68	3.0565	6 1 0	24	2.1301	5 6 1
11	3.0171	4 3 1	7	2.0137	4 8 0
11	2.9637	0 5 1	31	1.9911	6 6 1
22	2.8833	5 2 1	16	1.9796	7 5 1
28	2.8239	2 5 1	9	1.8769	7 0 2
10	2.7519	4 4 1	9	1.8504	10 1 0
"	"	6 3 0	"	"	8 5 1
9	2.7122	5 3 1	14	1.8302	8 6 0
41	2.6744	3 5 1	"	"	8 5 1
9	2.6234	1 0 2	8	1.7315	8 6 1
56	2.5716	1 6 1	"	"	7 4 2
"	"	6 2 1	7	1.6301	9 0 2
38	2.5489	2 0 2	13	1.6177	9 6 1
50	2.5008	2 6 1	14	1.6007	2 1 1 0
"	"	4 5 1	13	1.5834	0 5 3
17	2.4365	3 0 2	11	1.5784	1 5 3

amphibole to record a representative X-ray powder pattern. Thus, we collapsed the single-crystal X-ray intensity data to produce an experimental two-dimensional diffraction pattern that simulates that of a powder pattern (Table 3) in much the same way as a Gandolfi camera.

Crystal-structure refinement

A crystal was attached to a tapered glass fiber and mounted on a Bruker D8 three-circle diffractometer equipped with a rotating-anode generator (MoK α radiation), multilayer optics, and an APEX-II detector. A total of 22 604 intensities was collected to 65° 2 θ using 6 s per 0.3° frame, with a crystal-to-detector distance of 5 cm. Empirical absorption corrections (SADABS; Sheldrick 2008) were applied and equivalent reflections were corrected for Lorentz, polarization and background effects, averaged and reduced to structure factors. The unit-cell dimensions were obtained by least-squares refinement of the positions of 4043 reflections with $I > 10\sigma I$ and are given in Table 4, together with other information pertaining to data collection and structure refinement. All calculations were done with the SHELXTL PC (Plus) system of programs; *R* indices are given in Table 4 and are expressed as percentages. The structure was refined to con-

TABLE 4. Miscellaneous information for ferro-papikeite

<i>a</i> (Å)	18.628(4)	Crystal size (µm)	30 × 40 × 50
<i>b</i>	17.888(4)	Radiation/monochromator	MoKα/graphite
<i>c</i>	5.3035(11)	No. unique reflections	2941
<i>V</i> (Å ³)	1767.2(6)	No. <i>I</i> ₀ >4σ _I	2335
Space group	<i>Pnma</i>	<i>R</i> _{merge} %	3.80
<i>Z</i>	4	<i>R</i> _{obs} %	3.60
<i>D</i> _{calc} (g/cm ³)	3.488	<i>R</i> _{all} %	4.83

TABLE 5. Selected interatomic distances (Å) in ferro-papikeite

T1A–O1A	1.680(3)	T1B–O1B	1.691(3)	
T1A–O5A	1.680(3)	T1B–O5B	1.699(3)	
T1A–O6A	1.661(3)	T1B–O6B	1.680(3)	
T1A–O7A	1.656(1)	T1B–O7B	1.668(2)	
<T1A–O>	1.669	<T1B–O>	1.685	
T2A–O2A	1.630(2)	T2B–O2B	1.672(3)	
T2A–O4A	1.612(2)	T2B–O4B	1.646(2)	
T2A–O5A	1.650(3)	T2B–O5B	1.675(3)	
T2A–O6A	1.618(2)	T2B–O6B	1.662(2)	
<T2A–O>	1.628	<T2B–O>	1.664	
M1–O1A	2.070(3)	M2–O1A	1.977(3)	
M1–O1B	2.072(2)	M2–O1B	1.972(3)	
M1–O2A	2.195(2)	M2–O2A	1.978(3)	
M1–O2B	2.200(2)	M2–O2B	1.990(3)	
M1–O3A	2.122(2)	M2–O4A	1.901(2)	
M1–O3B	2.094(2)	M2–O4B	1.919(3)	
<M1–O>	2.126	<M2–O>	1.956	
M3–O1A	2.144(3)	x2	M4–O2A	2.265(2)
M3–O1B	2.162(2)	x2	M4–O2B	2.137(2)
M3–O3A	2.068(3)		M4–O4A	2.144(3)
M3–O3B	2.068(4)		M4–O4B	2.034(2)
<M3–O>	2.125		M4–O5A	2.226(2)
			M4–O5B	2.367(3)
			<M4–O>	2.196
A1–O6A	2.676(4)	x2	A2–O6A	2.50(2)
A1–O6B	2.626(5)	x2	A2–O7A	2.80(5)
A1–O7A	2.435(6)		A2–O7B	2.83(4)
A1–O7B	2.393(5)		A2–O7B	2.37(4)
<A1–O>	2.572		<A2–O>	2.60
A1–A2	1.15(6)			
O3A–HA	0.963		HA–O6A	2.673
			HA–A2	2.079
O3B–HB	0.961		HB–O6B	2.432

vergence by full-matrix least-squares methods with anisotropic-displacement parameters for all atoms except the H atoms HA and HB. At the later stages of refinement, difference-Fourier maps showed weak density maxima approximately 1 Å from the O3A and O3B anions. These maxima were entered into the structure model as H atoms and their positional parameters were refined with the soft constraint that the O3A–HA and O3B–HB distances be ~0.96 Å. The structure converged to a final *R*_{obs} index of 3.60%. Selected interatomic distances are given in Table 5, refined site-scattering values (Hawthorne et al. 1995) are listed

TABLE 7. Bond-valence (v.u.)^a table for ferro-papikeite

	M1	M2	M3	M4	T1A	T1B	T2A	T2B	A1	A2	HA	HB	Σ
O1A	0.385	0.429	0.330 ^{x21}		0.875								2.019
O1B	0.383	0.435	0.316 ^{x21}			0.852							1.986
O2A	0.291	0.429		0.254			0.986						1.960
O2B	0.328	0.416		0.339				0.892					1.975
O3A	0.343		0.391 ^{x2→}								0.90		2.025
O3B	0.365		0.391 ^{x2→}									0.85	1.997
O4A		0.522		0.334			1.032						1.888
O4B		0.499		0.463				0.954					1.916
O5A				0.278	0.975		0.937						2.190
O5B				0.202		0.835		0.885					1.922
O6A					0.919		1.017		0.062 ^{x21}	0.009 ^{x21}	0.10		2.107
O6B						0.877		0.915	0.070 ^{x21}	0.004 ^{x21}		0.15	2.016
O7A					0.930 ^{x2→}				0.110	0.006			1.976
O7B						0.904 ^{x2→}			0.121	0.012			1.941
Σ	2.095	2.730	2.074	1.870	3.699	3.528	3.972	3.646	0.495	0.044	1	1	

Note: ^a Bond-valence parameters from Gagné and Hawthorne (2015).

TABLE 6. Site populations (apfu) for ferro-papikeite

Site	R _{ss} ^a	Assigned site population (apfu)
T1A	–	0.75 Al + 1.25 Si
T1B	–	0.92 Al + 1.08 Si
T2A	–	0.06 Al + 1.94 Si
T2B	–	0.67 Al + 1.33 Si
M1	44.0(4)	0.58 Mg + 1.42 Fe ²⁺
M2	28.4(3)	0.21 Mg + 0.16 Fe ³⁺ + 0.01 Ti + 1.62 Al
M3	23.4(2)	0.19 Mg + 0.81 Fe ²⁺
M4	49.2(4)	0.20 Mg + 1.80 Fe ²⁺
A1	6.7(1)	0.64 Na
A2	0.6(1)	0.06 Na

^a Refined site-scattering factors (Hawthorne et al. 1995).

in Table 6, and a bond-valence table is given in Table 7. Refined atom coordinates and anisotropic-displacement parameters (Online Materials¹ Table OM1), a table of structure factors, and a Crystallographic Information File (CIF¹) for ferro-papikeite.

DERIVATION OF SITE POPULATIONS

Site populations were derived from the results of EMP analysis (Table 2) and structure refinement (Table 6), and the calculated bond-valences (Table 7). The refined <*T*–O> distances range from 1.628 to 1.685 Å (Table 5) and indicate the presence of appreciable Al at the *T* sites, in accord with the chemical formula (Table 2). Hawthorne et al. (2008) gave equations relating <*T*–O> distances to [⁴¹Al] site-populations for the individual tetrahedra in *Pnma* amphiboles; using these equations in conjunction with the observed <*T*–O> distances (Table 5) gives site populations that sum to [⁴¹Al]: 2.51 apfu, reasonably close to the value for [⁴¹Al] obtained by chemical analysis: 2.40 apfu (Table 2). The values obtained from the observed distances were proportionately decreased to accord with the bulk composition of the crystal.

The [⁶¹Al] was assigned to the *M2* site as the *M2* octahedron has the shortest mean bond length of the *M* polyhedra (Table 5) in accord with occupancy by Al³⁺, the smallest C-cation in papikeite. The *M1*, *M3*, *M4*, and remaining *M2* site populations were refined, and the site-scattering values (Hawthorne et al. 1995) are given in Table 6. Hawthorne et al. (2008) gave equations relating <*M*–O> distances to the aggregate radius of the ions occupying each *M*-site; the predicted values are close to the observed values for all three sites (Table 8), the values for *M2* supporting the assigned amount of Fe³⁺. As expected, Fe²⁺ is strongly ordered at the *M4* site relative to Mg²⁺ (Table 6).

TABLE 8. Observed and calculated $\langle M-O \rangle$ distances (Å) and aggregate cation radii (Å) in ferro-papikite

	$\langle M-O \rangle_{\text{obs}}$	$\langle M-O \rangle_{\text{calc}}$
$\langle M1-O \rangle$	2.126	2.122
$\langle M2-O \rangle$	1.956	1.954
$\langle M3-O \rangle$	2.125	2.116

THE VALENCE-SUM RULE AS A DRIVER OF STEREOCHEMICAL VARIATION IN FERRO-PAPIKEITE

The bond-valence table (Table 7) shows that the incident bond-valence sums at the sites in the structure accord closely with the valence-sum rule (Brown 2016; Hawthorne 2012, 2015) with a root-mean-square deviation of 0.08 v.u., indicating that the cations in the structure order to minimize these deviations. Of particular note are the O4A and O4B anions, which are [3]-coordinated and link to cations at $M2$, $M4$, $T2A$, and $T2B$. The incident Pauling bond-strength sums at O4A and O4B are 0.33/0.50 + 0.25 + 0.75/1.00, ranging from 1.33 to 1.75 v.u., depending on the occupancies of the $M2$, $M2$, $T2A$, and $T2B$ sites. To accord with the valence-sum rule, trivalent cations (i.e., Al^{3+} and Fe^{3+}) need to order at the $M2$ site, and tetravalent cations (i.e., Si^{4+}) need to order at the $T2A$ and $T2B$ sites, and that is the order that we see in Table 6. However, even with this optimum state of order, the incident bond-strengths are still only 1.75 v.u., and hence the bond lengths to O4A and O4B also need to be shorter than the other bonds to these cations. This is what occurs (Table 5): $\langle M2-O4A, O4B \rangle = 1.910$ Å; $\langle M2-O1A, O1B, O2A, O2B \rangle = 1.979$ Å; $\langle M4-O4A, O4B \rangle = 2.089$ Å; $\langle M4-O2A, O2B, O5A, O5B \rangle = 2.249$ Å; $\langle T2A-O4A, T2B-O4B \rangle = 1.629$ Å; $\langle T2A-O2A, O5A, O6A, T2B-O2B, O5B, O6B \rangle = 1.651$ Å.

One unexpected feature of ferro-papikite is the presence of two well-resolved A sites separated by 1.15(6) Å with Na very strongly ordered at the $A1$ site (Table 6). Inspection of Table 5 gives us a clue as to the origin of this site splitting. The $A1-O7A$ distance is quite short, 2.435 Å, in line with the gedrites refined by Schindler et al. (2008), whereas the $A2-O7A$ distance is much longer, 2.843 Å. Thus, Na at $A2$ provides less bond-valence to O7A than Na at $A1$. This suggests that Na at $A1$ preferentially bonds to O7A involved in a ${}^{T1A}Si-O7A-{}^{T1A}Al$ linkage, whereas Na at $A2$ bonds to O7A involved in a ${}^{T1A}Si-O7A-{}^{T1A}Si$ linkage

(as does ${}^4\Box$). The H^+ ions HA and HB hydrogen-bond to the corresponding O6A and O6B anions. Note that HA is too close to $A2$ (Table 5), which suggests that the occurrence of Na at $A2$ may be locally associated with a small amount of F at O3A, in accord with the amount of F detected during electron-microprobe analysis (Table 2).

DISCUSSION

The ideal formula of the amphibole species reported here is $NaFe_2^{2+}(Fe_3^{2+}Al_2)(Si_5Al_3)O_{22}(OH)_2$. Examination of the relevant classification diagram of Hawthorne et al. (2012) shows that this formula corresponds to the Fe^{2+} -equivalent of Rootname 2. A new rootname has been approved for this amphibole species: ferro-papikite. Figure 3a shows the current nomenclature status of the $Pnma$ amphiboles with the composition of ferro-papikite shown by the red circle; amphibole compositions corresponding to Rootname 1 have yet to be described as a new mineral species.

IMPLICATIONS

Figure 3b shows chemical variations in selected $Pnma$ amphiboles. The amphiboles of Schindler et al. (2008) (pale-brown circles in Fig. 3b) define a well-developed linear relation passing close to the ideal composition $Na_{0.5}M_2^{2+}(M_{3.5}^{2+}M_{1.5}^{3+})(Si_6Al_2)O_{22}(OH)_2$ (where $M^{2+} = Mg^{2+}, Fe^{2+}$; $M^{3+} = Al^{3+}, Fe^{3+}$) defined by Robinson et al. (1971). These amphiboles and those characterized by Robinson et al. (1971) are from amphibolite-grade rocks. The amphiboles of Berg (1985) and Claeson and Meurer (2002), shown by green and yellow circles, respectively, in Figure 3b, lie far off the linear relation shown in Figure 3b, being greatly enriched in Na relative to most of the other orthorhombic amphiboles. The amphiboles of Berg (1985) occur in a xenolith of ferro-aluminous gneiss within a granite, and those of Claeson and Meurer (2002) occur in a troctolite cumulate. It seems that high temperatures promote the incorporation of Na into the $Pnma$ amphibole structure. Although ferro-papikite contains significantly more Na than the amphiboles of Robinson et al. (1971) and Hawthorne et al. (2008), it lies close to the trend line for amphiboles from amphibolite-grade rocks, in accord with its metamorphic origin.

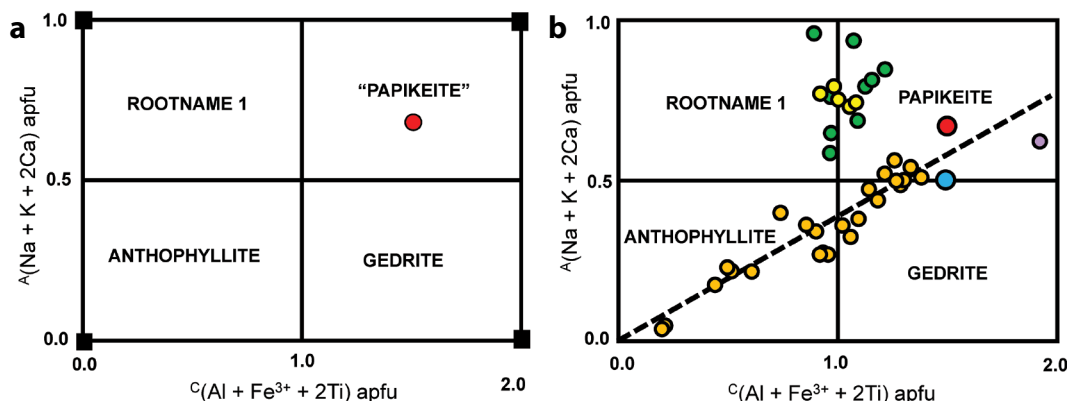


FIGURE 3. (a) Orthorhombic magnesium-iron-manganese amphiboles and their compositional boundaries. Filled black squares are the locations of named and unnamed root compositions; ferro-papikite is shown by the red circle. (b) Chemical variations in selected $Pnma$ amphiboles: data of Schindler et al. (2008) (pale-brown circles), Berg (1985) (green circles), Claeson and Meurer (2002) (yellow circles), and Schreyer et al. (1993) (small mauve circle); the large blue circle is the “ideal end” composition of Robinson et al. (1971), and the large red circle is ferro-papikite; the dashed line is drawn as a guide to the eye; modified from Hawthorne et al. (2008).

There are strong similarities between the distribution of chemical compositions for both *Pnma* and *C2/m* (Robinson et al. 1971) amphiboles. For the *Pnma* amphiboles, there is a lack of compositions corresponding to Rootname 1 (Fig. 3b). For the *C2/m* amphiboles, there is a similar lack of compositions corresponding to edenite although synthetic amphiboles can approach quite closely to the composition of fluoro-edenite (e.g., Boschmann et al. 1994; Oberti et al. 1997). There has been a considerable amount of work on fluoro-edenite (e.g., Gianfagna and Oberti 2001; Gianfagna et al. 2007; Della Ventura et al. 2014), particularly because of its importance as an environmental cause of malignant pleural mesothelioma (Paoletti et al. 2000; Comba et al. 2003). It is of significance to understand the crystal-chemical constraints on the occurrence of amphibole compositions in the fields of edenite and Rootname 1, as these may relate to the carcinogenic properties of fibrous fluoro-edenite.

ACKNOWLEDGMENTS AND FUNDING

We thank John Hughes and Gordon Brown, Jr. for their very good comments on this paper. We thank Alfredo Camacho, Department of Geological Sciences, University of Manitoba, for arranging for thin sections to be cut, and for help with the thin-section photography and interpretation. This work was supported by a Natural Sciences and Engineering Research Council of Canada Discovery Grant, and by Canada Foundation for Innovation grants to F.C.H.

REFERENCES CITED

- Bartelmeis, K.L., Bloss, F.D., Downs, R.T., and Birch, J.B. (1992) Excalibr II. Zeitschrift für Kristallographie, 199, 185–196.
- Berg, J.H. (1985) Chemical variation in sodium gedrite from Labrador. American Mineralogist, 70, 1205–1210.
- Boschmann, K., Burns, P.C., Hawthorne, F.C., Raudsepp, M., and Turnock, A.C. (1994) A-site disorder in synthetic fluoro-edenite, a crystal structure study. Canadian Mineralogist, 32, 21–30.
- Brown, I.D. (2016) The Chemical Bond in Inorganic Chemistry. The Bond Valence Model, 2nd ed. Oxford University Press.
- Claeson, D.T., and Meurer, W.P. (2002) An occurrence of igneous orthorhombic amphibole, Eriksberg gabbro, southern Sweden. American Mineralogist, 87, 699–708.
- Comba, P., Gianfagna, A., and Paoletti, L. (2003) Pleural mesothelioma cases in Biancavilla are related to a new fluoro-edenite fibrous amphibole. Archives of Environmental Health, 58, 229–232.
- Della Ventura, G.D., Bellatreccia, F., Cámara, F., and Oberti, R. (2014) Crystal-chemistry and short-range order of fluoro-edenite and fluoro-pargasite: a combined X-ray diffraction and FTIR spectroscopic approach. Mineralogical Magazine, 78, 293–310.
- Gagné, O., and Hawthorne, F.C. (2015) Comprehensive derivation of bond-valence parameters for ion pairs involving oxygen. Acta Crystallographica, B71, 562–578.
- Gianfagna, A., and Oberti, R. (2001) Fluoro-edenite from Biancavilla (Catania, Sicily, Italy): Crystal chemistry of a new amphibole end-member. American Mineralogist, 86, 1489–1493.
- Gianfagna, A., Andreozzi, G.B., Ballirano, P., Mazziotti-Tagliani, S., and Bruni, B.M. (2007) Structural and chemical contrasts between prismatic and fibrous fluoro-edenite from Biancavilla, Sicily, Italy. Canadian Mineralogist, 45, 249–262.
- Hawthorne, F.C. (2012) A bond-topological approach to theoretical mineralogy: crystal structure, chemical composition and chemical reactions. Physics and Chemistry of Minerals, 39, 841–874.
- (2015) Toward theoretical mineralogy: a bond-topological approach. American Mineralogist, 100, 696–713.
- Hawthorne, F.C., and Oberti, R. (2007) Amphiboles: Crystal chemistry. In F.C. Hawthorne, R. Oberti, G. Della Ventura, and A. Mottana, Eds., Amphiboles: Crystal Chemistry, Occurrence and Health Issues, 67, p. 1–54. Reviews in Mineralogy and Geochemistry, Mineralogical Society of America, Chantilly, Virginia.
- Hawthorne, F.C., Ungaretti, L., and Oberti, R. (1995) Site populations in minerals: terminology and presentation of results of crystal-structure refinement. Canadian Mineralogist, 33, 907–911.
- Hawthorne, F.C., Schindler, M., Abdu, Y., Sokolova, E., Evans, B.W., and Ishida, K. (2008) The crystal chemistry of the gedrite-group amphiboles. II. Stereochemistry and chemical relations. Mineralogical Magazine, 72, 731–745.
- Hawthorne, F.C., Oberti, R., Harlow, G.E., Maresch, W., Martin, R.F., Schumacher, J.C., and Welch, M.D. (2012) Nomenclature of the amphibole super-group. American Mineralogist, 97, 2031–2048.
- Lagerblad, B., and Gorbatschev, R. (1985) Hydrothermal alteration as a control of regional geochemistry and ore formation in the central Baltic Shield. Geologische Rundschau, 74, 33–49.
- Le Maitre, R.W. (1976) The chemical variability of some common igneous rocks. Journal of Petrology, 17, 589–585.
- Leake, B.E. (1978) Nomenclature of amphiboles. Mineralogical Magazine, 42, 533–563.
- Linthout, K. (1983) From rhyolites to quartz-phlogopite-muscovite-schists: Proterozoic two-stage sub-seafloor alteration, W. Bergslagen, Sweden (abstract). Terra Cognita, 3, 179–180.
- Linthout, K., and Lustenhouwer, W.J. (1996) Subsilicic sodium gedrite in lepite of quartz keratophytic origin, Nordmark (Sweden). Mineralogical Magazine, 60, 379–387.
- Magnusson, N.H. (1970) The origin of the iron ores in central Sweden and the history of their alterations. Sveriges Geologiska Undersökning. Avhandlingar Och Uppsatsen, C, 643, 364p.
- Oberti, R., Hawthorne, F.C., and Raudsepp, M. (1997) The behaviour of Mn in amphiboles: Mn in synthetic fluoro-edenite and synthetic fluoro-pargasite. European Journal of Mineralogy, 9, 115–122.
- Paoletti, L., Batisti, D., Bruno, C., Di Paola, M., Gianfagna, A., Mastrantonio, M., Nesti, M., and Comba, P. (2000) Unusually high incidence of malignant pleural mesothelioma in a town of eastern Sicily: An epidemiological and environmental study. Archives of Environmental Health, 55, 392–398.
- Papiké, J.J., and Ross, M. (1970) Gedrites: crystal structures and intracrystalline cation distributions. American Mineralogist, 55, 1945–1972.
- Pouchou, J.L., and Pichoir, F. (1985) 'PAP' $\phi(\rho Z)$ procedure for improved quantitative microanalysis. In J.T. Armstrong, Ed., Microbeam Analysis, p. 104–106. San Francisco Press, California.
- Rabbitt, J.C. (1948) A new study of the anthophyllite series. American Mineralogist, 33, 263–323.
- Robinson, P., and Jaffe, H.W. (1969) Chemographic exploration of amphibole assemblages from central Massachusetts and southwestern New Hampshire. Mineralogical Society of America Special Paper, 2, 251–274.
- Robinson, P., Ross, M., and Jaffe, H.W. (1971) Composition of the anthophyllite-gedrite series, comparisons of gedrite-hornblende, and the anthophyllite-gedrite solvus. American Mineralogist, 56, 1004–1041.
- Roep, T., and Linthout, K. (1989) Precambrian storm wave-base deposits of Early Proterozoic age (1.9 Ga), preserved in andalusite-cordierite-rich granofels and quartzite (Rämsberg area, Värmland, Sweden). Sedimentary Geology, 61, 239–251.
- Ross, M., Papiké, J.J., and Shaw, K.W. (1969) Exsolution textures in amphiboles as indicators of subsolidus thermal histories. Mineralogical Society of America Special Paper, 2, 275–299.
- Schindler, M., Sokolova, E., Abdu, Y., Hawthorne, F.C., Evans, B.W., and Ishida, K. (2008) The crystal chemistry of the gedrite-group amphiboles. I. Crystal structure and site populations. Mineralogical Magazine, 72, 703–730.
- Schreyer, W., Bernhardt, H.-J., and Medenbach, O. (1993) Ferrogedrite, siderophyllite, septechamosite, andalusite and chloritoid as alteration products of sekaninaite (ferrocordierite) from the Dolní Bory Pegmatite, Moravia. Russian Geology and Geophysics, 34, 125–131.
- Sheldrick, G.M. (2008) A short history of SHELX. Acta Crystallographica, A64, 112–122.
- Spear, F.S. (1993) Metamorphic Phase Equilibria and Pressure-Temperature-Time-Paths, 799 p. Monograph, Mineralogical Society of America, Chantilly, Virginia.
- Stout, J.H. (1971) Four coexisting amphiboles from Telemark, Norway. American Mineralogist, 56, 212–224.
- Vallance, T.G. (1967) Mafic rock alteration and isochemical development of some cordierite-anthophyllite rocks. Journal of Petrology, 8, 84–96.

MANUSCRIPT RECEIVED OCTOBER 31, 2020

MANUSCRIPT ACCEPTED FEBRUARY 4, 2021

MANUSCRIPT HANDLED BY PAOLO LOTTI

Endnote:

¹Deposit item AM-22-27877, Online Materials. Deposit items are free to all readers and found on the MSA website, via the specific issue's Table of Contents (go to http://www.minsocam.org/MSA/AmMin/TOC/2022/Feb2022_data/Feb2022_data.html). The CIF has been peer reviewed by our Technical Editors.